Thickness Uniformity of Uranium Oxide Films Sputtered While

Undergoing Planetary Motion

Jordan W. Bell

A senior thesis submitted to the faculty of
Brigham Young University
in partial fulfillment of the requirements for the degree of

Bachelor of Science

David D. Allred, Advisor

Department of Physics and Astronomy

Brigham Young University

December 2012

ABSTRACT

Thickness Uniformity of Uranium Oxide Films Sputtered While
Undergoing Planetary Motion

Jordan W. Bell
Department of Physics and Astronomy
Bachelor of Science

The thickness uniformity of thin films across a substrate's surface is of interest in many important applications, including the manufacture of multilayer mirrors and antireflective coatings. This thesis explores the thickness profile of films deposited by DC magnetron sputtering on large stationary substrates, then uses that data in a computer model to predict thickness uniformity for substrates undergoing "planetary" motion. We tested the ability of the model to make predictions by producing a sample under planetary rotation and measuring its thickness profile. We found that the model gave a good approximation to the actual thickness profile, but actually underestimated the thickness uniformity.

ACKNOWLEDGMENTS

Contents

Chapter 1

Introduction

Thin films are useful only to the extent that they can be controlled and characterized. Films of specified thickness and composition find useful applications in many fields from optics to microchips. Often, it is the thickness and refractive index of the film itself that gives the desired property. Such is the case with dielectric mirrors and antireflective coatings, which must contain multiple layers of various materials, deposited to within precise fractions of the wavelength of light. Matthew Squires's senior thesis gives a good treatment of the basic theory behind this. (Squires 1999)

Some groups in the past have attempted to study the deposition profile of sputtered material. (Wehner & Rosenberg 1960) No doubt there are also many specialized studies within industry, where vast amounts of money are at stake. While some aspects of the sputtering process are universal, there is a very large dependence on the specific geometry of the sputter system.

For our group's work in extreme ultraviolet (EUV or XUV), film uniformity takes on enormous importance because of the short (1-100 nm) wavelengths we use. This level of uniformity is very difficult to acheive. To make progress in the direction of thickness uniformity, we designed and installed a special roatating sample holder in our sputtering vacuum chamber. We sputtered several films of uranium oxide over samples spanning most of the chamber. (Heavy elements and their compounds are used because of their ability to reflect short wavelength readiation when deposited

in layers with a less dense spacer, such as silicon.) Using data obtained from these preliminary samples, we built a computer model and used it to predict film uniformity for samples produced with the new sample holder. We then made a film using the new sample spinning system to test our predictions.

Chapter 2

Experimental Methods and Results

Sputtering naturally produces a plume of material which results in a deposition profile which is uneven, but symmetrically centered about the axis of the sputtering target. An example of this is given in Figure 2.1. In order to avoid the nonuniformity of this natural deposition, we developed a substrate holder which would allow our samples to follow "planetary motion," meaning that the sample would revolve around the center of the vacuum chamber while rotating about the axis of the sample holder, in much the same way that the earth rotates around its own axis while revolving around the sun.

This was designed so that each point on the substrate would spend time in as many locations within the deposition plume as possible, thus providing an averaging effect. If one half of the substrate was facing the greatest particle flux and given a thick deposition layer, the next moment it would find itself in an area of less flux, and the layer across the whole sample would become uniform once more. We developed a computer program (Section 2.3) to predict the thickness uniformity across the sample given the static deposition profile. In order to measure the static deposition profile across the entire chamber, I constructed large substrates from arrays of glass microscope slides. I made three different samples (Arrays 1, 2, and 3), allowing us to measure the sputtering profile with the sputter gun different distances from the substrate. The film thicknesses were mea-
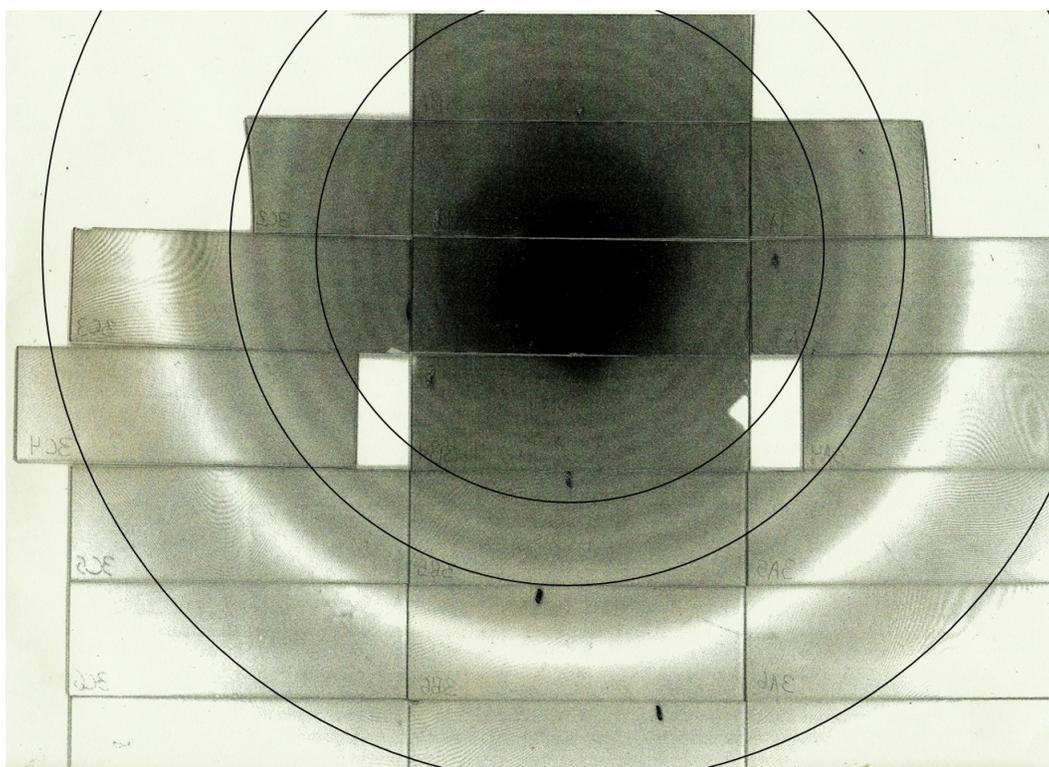
Figure 2.1 A photocopy of part of Slide Array 3 showing interference fringes associated with varying film thicknesses. Circles are superimposed to call attention to the approximately circular symmetry of the deposition pattern.

sured with spectroscopic ellipsometry, using a J.A. Woolam XLS-100 ellipsometer. These values were then fed into the computer program, which provided the sputtering parameters to use for optimal film-thickness uniformity. I then sputtered another film in accordance with these optimal parameters, followed by ellipsometric characterization.

2.1   Apparatus

2.1.1   Sputtering Chamber

Our samples were prepared in a cylindrical vacuum chamber measuring approximately 11.5 inches across the interior diameter and 15 inches top to bottom. The chamber is fitted with three MeiVac MAK sputter guns (two 4-inch size and one 2-inch size) which can be raised and lowered within the chamber. The center of the 4-inch gun we used was offset from the center of the chamber by approximately 3 3/8 inches. The chamber is fitted with a CTI-Cryogenics Cryo-Torr 8 Helix High Vacuum Cryopump as well as a varian TV141 Navigator turbopump, allowing our baseline pressures to drop into the microtorr level. Pressures were measured with a thermocouple gauge down to the millitorr range, and an ion gauge for lower pressures.

2.1.2   Planetary Apparatus

As shown in Fig. 2.2, the 4.5-inch diameter sample holder is suspended from an axis in the center of the chamber by a cantilever system which allows for planetary motion. The entire apparatus is attached to an axle through the center of the top of the chamber, enabling it to revolve around the axis of the chamber. The sample holder is attached to a smaller axle set in bearings, offset from the revolution axis by 2.87 inches.

The sample holder is made to rotate by an o-ring attached to the other end of the rotation axle. This o-ring engages a smooth cylinder "track" set into the ceiling of the vacuum chamber. A pair
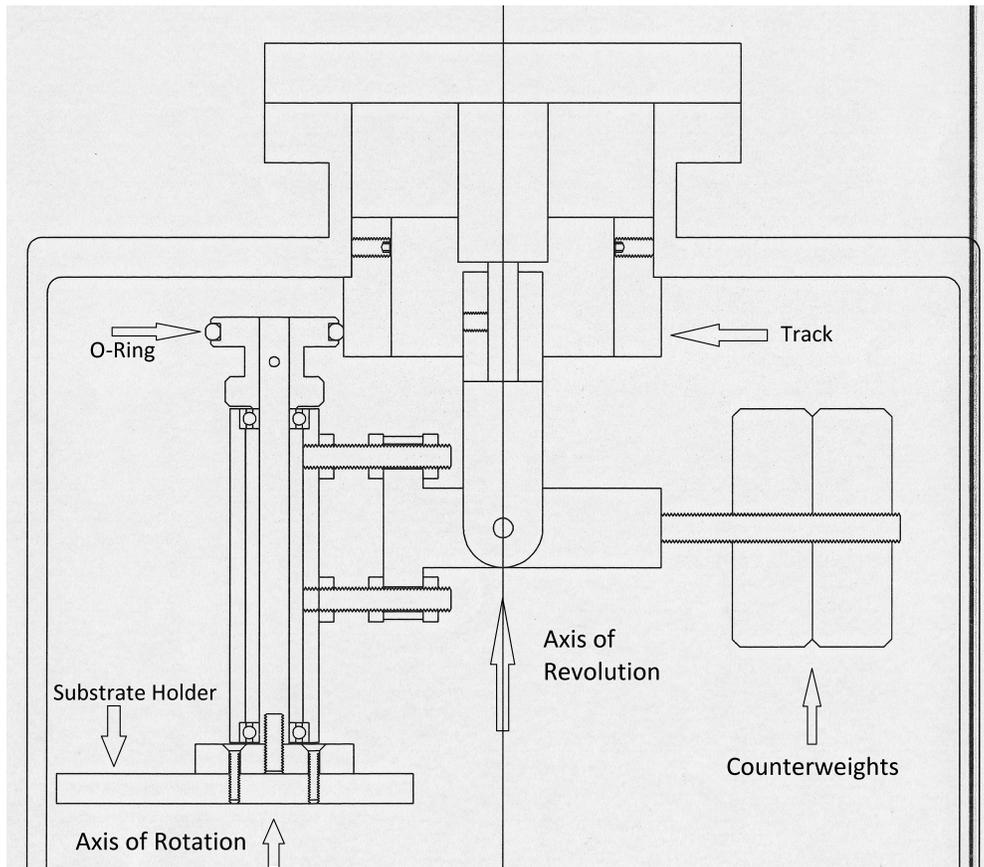
Figure 2.2 A cut-away diagram of the planetary apparatus.

of counterweights attached to the other end of the apparatus encourages the o-ring to engage this cylinder, but because the cylinder is smooth, the result is a loose coupling, in which the o-ring occasionally slips. The o-ring's diameter is 1:2.26 that of the cylinder it follows.

The final version of this planetary system was designed and constructed by Wesley Lifferth, the BYU Physics Department Machinist and Design Engineer.

2.1.3 Substrate Array

In order to determine the sputtering profile, we needed to make a single deposition while capturing sputtered material across as much of the 11.5-inch vacuum chamber as possible. This was difficult
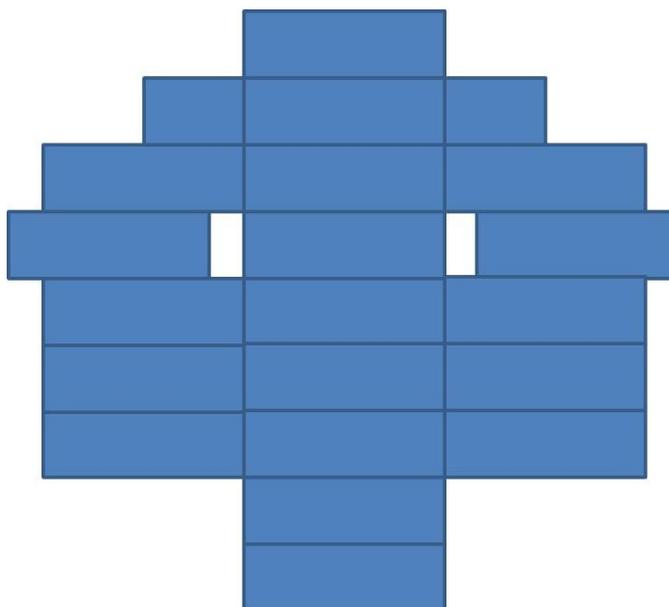
Figure 2.3 A top view of the arrangement of the entire substrate array.

because the chamber's door measures only 6 inches across, making use of a large single substrate impossible.

To cope with this difficulty, I devised an array of standard glass microscope slides (VWR Vistavision 16004-424, ISO 8037/1), held together only by Kapton tape on the side facing the top of the chamber. The tension in this vacuum-compatible, heat-resistant tape counters the tendency of the array to buckle under its own weight. Each slide measures 1 by 3 inches, and is 1.2 mm thick. Each array consists of 20 such slides (one broken in half) as shown in Fig. 2.3. Two of the slides are positioned 1/2 inch outward to allow the whole array to be secured to the sample holder by two clips and its own weight.

Held towards the middle, pressing up against the sample holder on one end, and suspended across the chamber on the other end, the array becomes rigid and may be treated essentially as one large piece of glass. It may be easily folded towards the taped side (see Fig. 2.4) and rolled up in order to fit through the chamber port.

On the tape side, the slides are labeled according to their position in the array. Film measure-
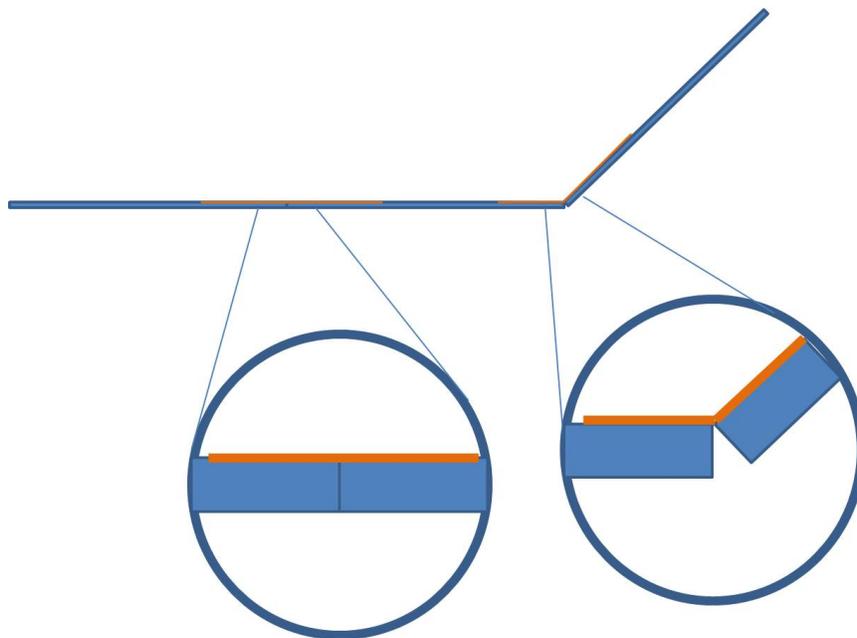
Figure 2.4 A close-up of the hinge mechanism illustrating tape and slide construction.

ments on individual slides can then be organized according to position within the chamber.

2.2 Deposition and Characterization

Three slide arrays were produced and used for UO_x deposition. Slide Array 1 was sputtered without enough oxygen and became opaque and useless for our purposes. Slide Array 2 and Slide Array 3 were used to characterize the profile of UO_x deposition.

2.2.1 Array 2

Sputtering Parameters

Slide Array 2 was sputtered (Feb. 11, 2012) with the uranium target placed slightly less than 5 inches away at the closest point. We brought the chamber to a baseline pressure of $2.5 * 10^{-6}$ torr. We then throttled the cryopump by partially closing the gate valve between it and the chamber,
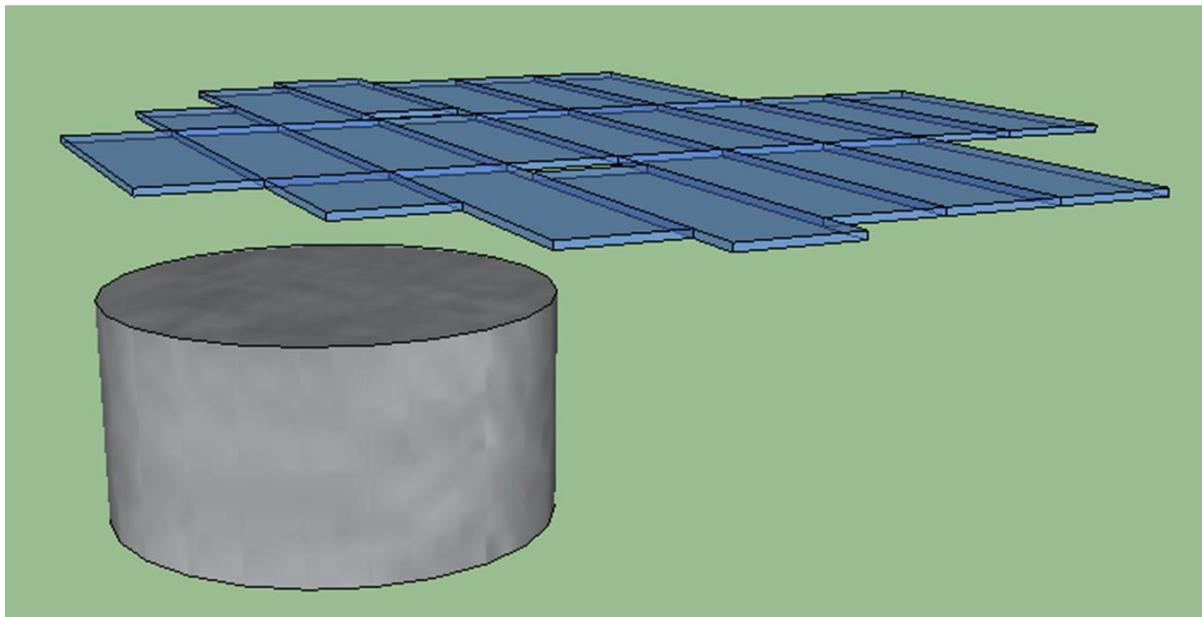
Figure 2.5 A view of the array's position relative to the target. This position is near that used for Array 3 (4 cm).

and the pressure rose to $3.0 * 10^{-6}$ torr. At this point we allowed oxygen to flow into the chamber (sapphire valve setting 4 11/12) until the pressure reached $3.1 * 10^{-4}$ torr. We then released argon into the chamber until the total pressure reached $1.5 * 10^{-3}$ torr. We switched off the turbopump and read the pressure at 1.6 to $1.7 * 10^{-3}$ torr. We turned on the plasma and found it to be a yellow color (unlike the usual blue for argon). The pressure held at around $5.2 * 10^{-3}$ torr. The plasma was sustained for 15 minutes, during which time the voltage between the target and the chamber rose from 581 volts to 624 volts. The current through the target fell from 0.6 amps to 0.56 amps during the same period.

When the plasma was turned off, we measured the chamber pressure at $2.8 * 10^{-3}$ torr. Here we discovered that when the argon was turned off, the pressure remained at 2.7 to $2.8 * 10^{-3}$ torr, while when we turned off the oxygen and left the argon on, the pressure dropped to $1.4 * 10^{-4}$ torr. We had sputtered in almost pure oxygen (95%).

We discovered that the cryopump had saturated and dumped its contents into the chamber (the
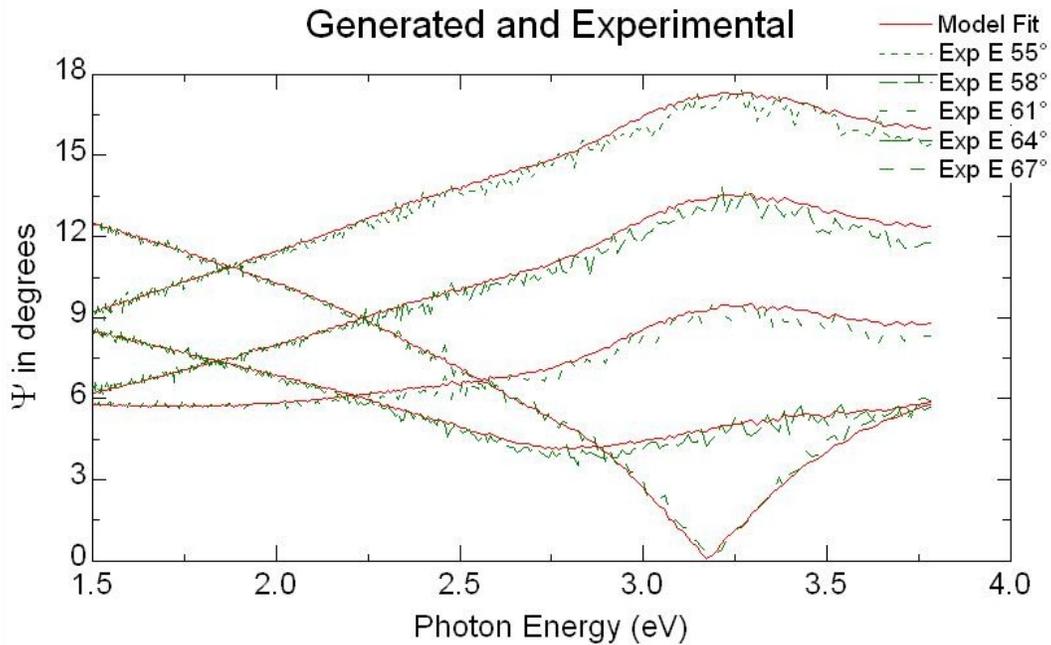
Figure 2.6 Ellipsometric measurement Ψ relative to photon energy (eV) for five angles for a point on Array 2.

pump's temperature had risen to 40 K). We believe that Argon's lower vapor pressure caused it to condense preferentially, leaving the higher percentage of oxygen in the chamber. We turned the turbopump back on and pumped out the cryopump for 30 minutes. It began at $1 * 10^{-2}$ torr, but eventually fell to $8 * 10^{-6}$ torr. We then removed the sample.

Characterization

We took tranmission measurements as well as multi-angle ellipsometric measurements at many points across Slide Array 2. Multiple datasets were used at once to constrain an optical model of the film as well as its thickness using J.A.Woolam's WVASE software. An example plot of ellipsometric data Ψ and the model fit is given in Fig. 2.6. Optical constants n and k as well as the dielectric constants ε_1 and ε_2 for the film material were obtained from the model and are
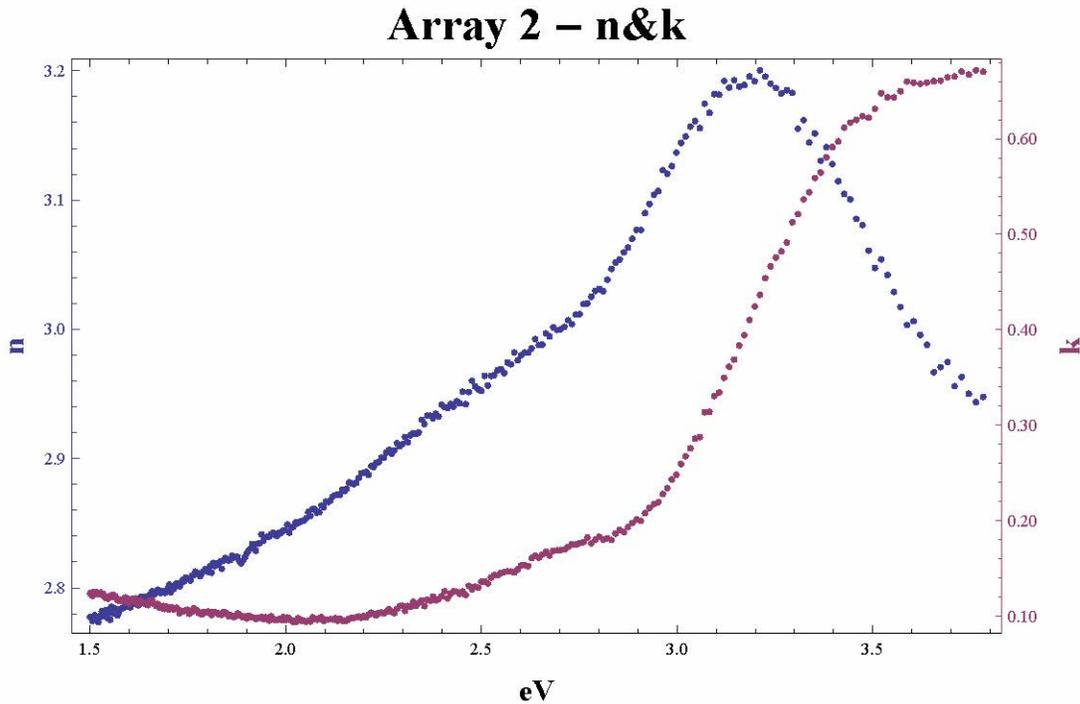
Figure 2.7 Optical constants n and k for Array 2 as a function of photon energy (eV).

given in Fig. 2.7 and Fig. 2.8 respectively. Figure 2.9 is a compilation of thicknesses at various points on the array. We located the center of the approximately symmetric thickness profile and give the thicknesses versus their radial distance from this point. Using some dummy points to help constrain the fit to suitable boundary conditions, the data was fit with a fifth-order polynomial shown. (This function was later used in making our computational model.)

2.2.2 Array 3

Sputtering Parameters

Slide Array 3 was sputtered (March 7, 2012) at approximately 4 cm from the uranium target. The chamber reached a base pressure of $2.5 * 10^{-6}$ torr before rising to $2.8 * 10^{-6}$ torr when the pumps were throttled. We then set the oxygen at 4 5/8, which raised the pressure to $3.1 * 10^{-4}$ torr. The
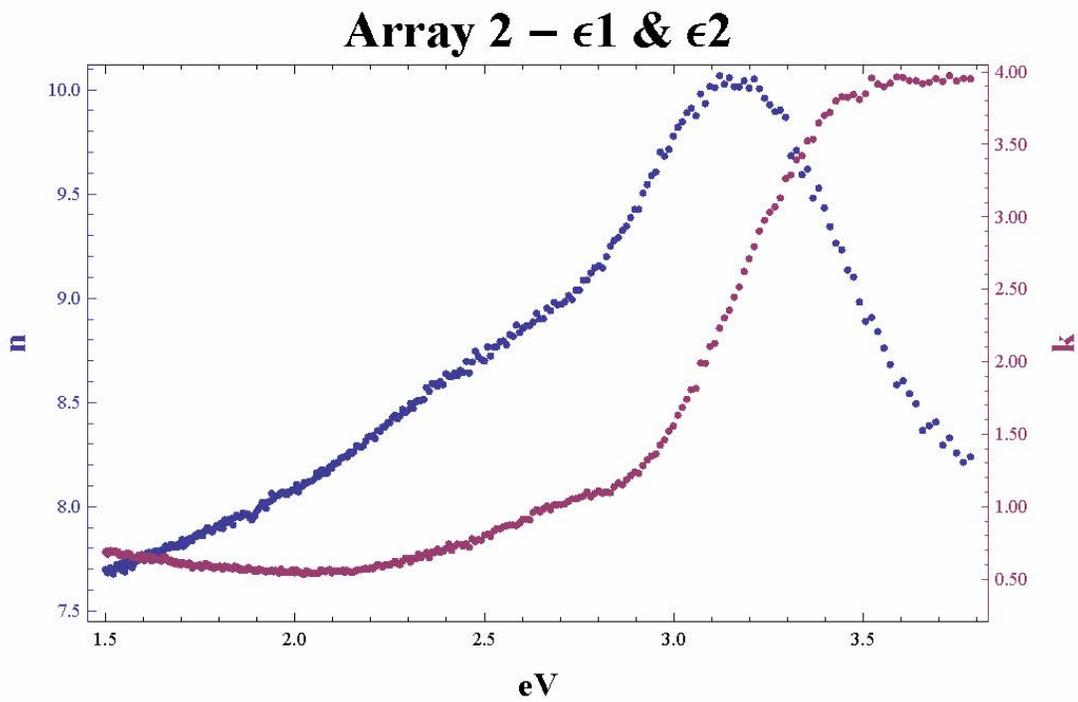
Figure 2.8 Dielectric constants ε_1 and ε_2 for Array 2 as a function of photon energy (eV).
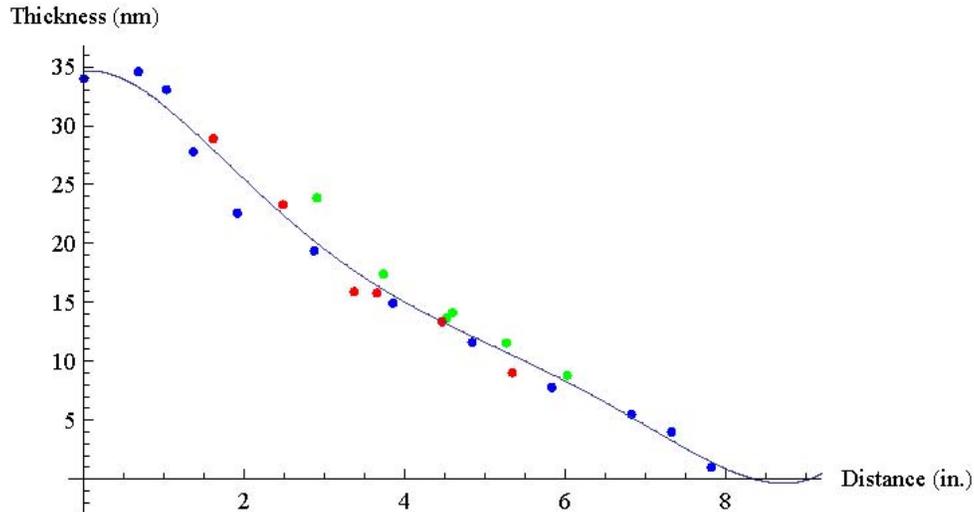

Figure 2.9 Array 2 film thickness as a function of radial distance from the center of the deposition profile. The blue points represent measurements taken along the symmetry axis of the array, while green and red points are those measured on either side. Also shown is a polynomial function fit of the data.

Mass Flow Controller (MFC) was turned to 1.4 for argon, leading to a pressure of $1.8 * 10^{-3}$ torr by the ion gauge.

We then ignited an argon-oxygen plasma, which was sustained at $1.8 * 10^{-3}$, but this was found to be somewhat unstable, so we lowered the pressure (setting 4 2/3) after about one minute total sputtering. Adjusting the MFC to 1.6 brought the pressure to $2.0 * 10^{-3}$ torr.

We sputtered for a total of 60 minutes, during which the voltage from chamber to target varied from 680 volts to 718 volts. The current through the target dropped from 0.52 amps to 0.49 amps. About five minutes into sputtering, the ion gauge measured a pressure of about 3.5 millitorr. At about 20 minutes of sputtering this pressure had dropped to 3.0 millitorr. These values are likely a bit high due to the effect of the plasma on the ion gauge.

When the plasma was turned off, the pressure was read at $1.8 * 10^{-3}$ torr. We turned off the argon flow which brought the pressure in the chamber to $3 * 10^{-4}$ torr. Turning off the oxygen returned the chamber to a 2.5 microtorr base pressure. We then vented the chamber and removed the sample.

Characterization

Slide Array 3 was characterized in the same way as Array 2 (Section 2.2.1). A representative plot of Ψ and the model fit is given in Fig. 2.10. Optical constants n and k as well as the dielectric constants ε_1 and ε_2 for the film material are given in Fig. 2.11 and Fig. 2.12. Figure 2.13 is a plot of film thickness as a function of radial distance similar to that given for Array 2 in Figure 2.9, only this time a ninth-order polynomial fit was used.
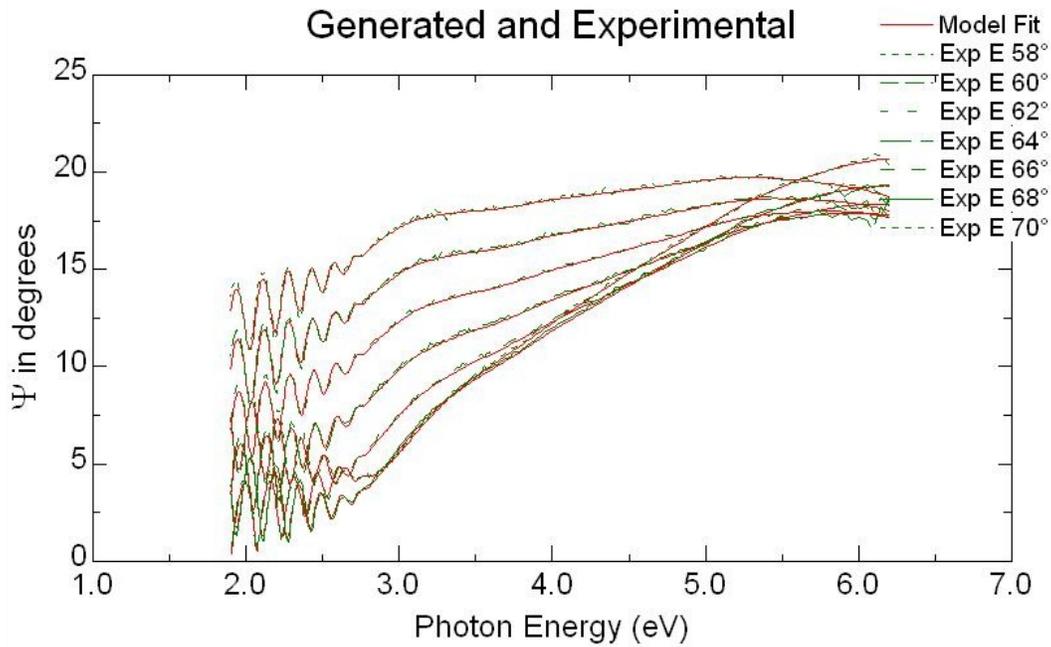
Figure 2.10 Ellipsometric measurement Ψ relative to photon energy (eV) for seven angles for a point on Array 3.
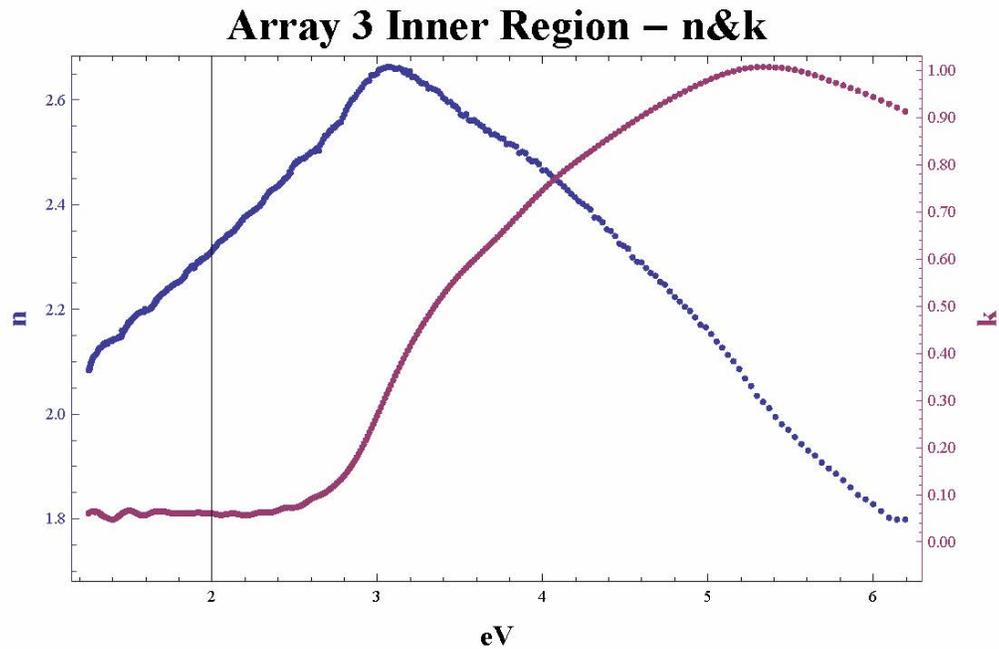
Figure 2.11 Optical constants n and k for Array 3 as a function of photon energy (eV).

Array 3 Inner Region − $\epsilon 1$ & $\epsilon 2$
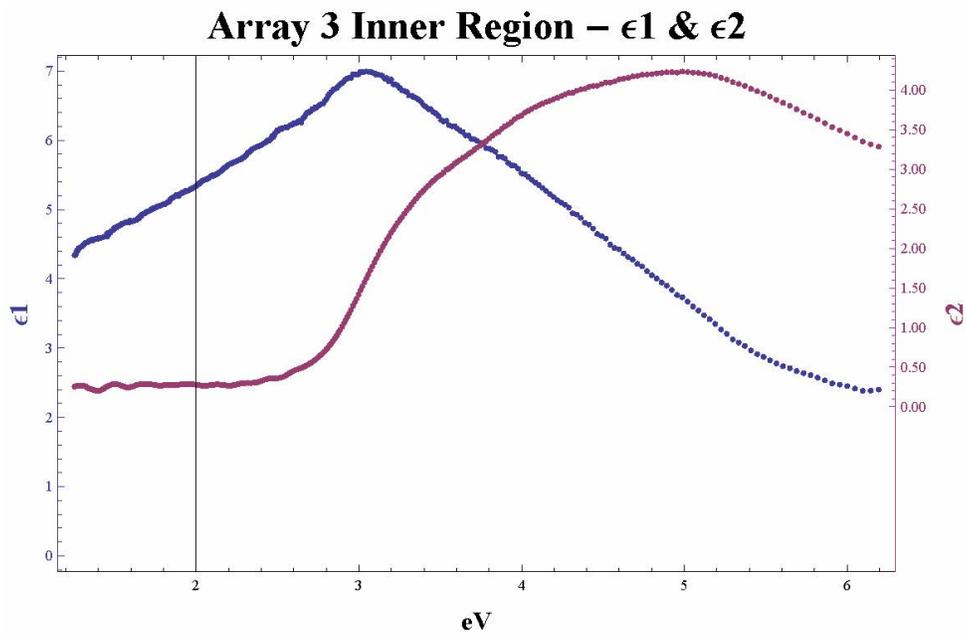
Figure 2.12 Dielectric constants ε_1 and ε_2 for Array 3 as a function of photon energy (eV).
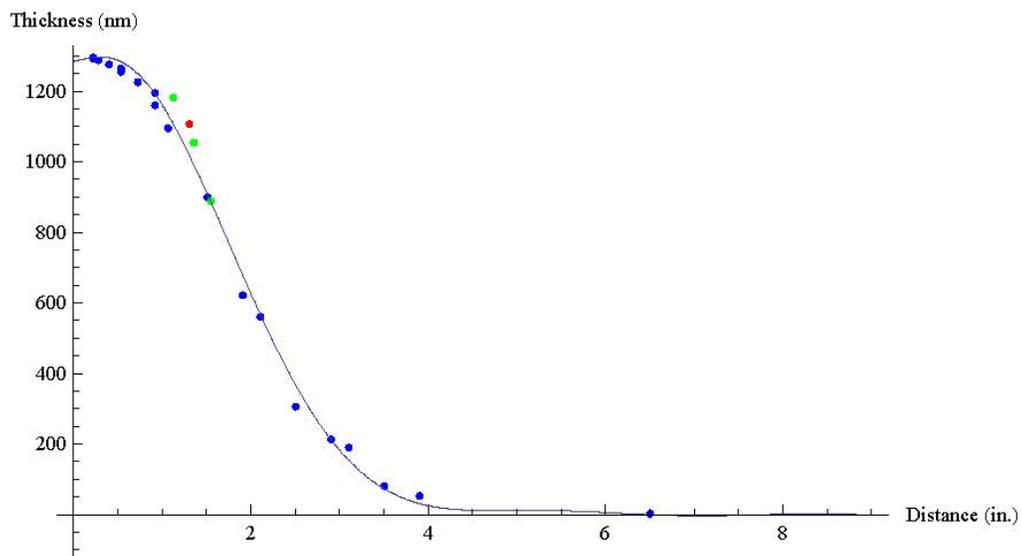
Figure 2.13 Array 3 film thickness as a function of radial distance from the center of the deposition profile. The blue points represent measurements taken along the symmetry axis of the array, while green and red points are those measured on either side. Also shown is a polynomial function fit of the data.

2.3   Computer Simulation

2.3.1   Theory

We wrote a computer simulation in order to predict the uniformity of a sample based on its size and the number of revolutions, and hence rotations, it might undergo in the sputtering chamber. The MATLAB code is given in Appendix A. The approach is based on integrating the sputtering flux intercepted by each point on the sample as it undergoes planetary motion, which can be described by a rotation matrix followed by a translation matrix followed by another rotation matrix, operating on the position vector of the point in question.

The position of a point on the substrate can be given by the vector:

$$r = \begin{pmatrix} x \\ y \\ 1 \end{pmatrix}.$$

$$(2.1)$$

The rotation of the substrate holder is accomplished by the rotation matrix:

$$R_2 = \begin{pmatrix} \cos(\omega_2 t) & -\sin(\omega_2 t) & 0 \\ \sin(\omega_2 t) & \cos(\omega_2 t) & 0 \\ 0 & 0 & 1 \end{pmatrix},$$

$$(2.2)$$

while the distance between the axis of rotation and the axis of revolution (a) is inserted via the translation matrix:

$$T = \begin{pmatrix} 1 & 0 & a \\ 0 & 1 & 0 \\ 0 & 0 & 1 \end{pmatrix},$$

$$(2.3)$$

and the revolution of the rotating substrate holder around the center of the chamber is given by:

$$R_1 = \begin{pmatrix} \cos(\omega_1 t) & -\sin(\omega_1 t) & 0 \\ \sin(\omega_1 t) & \cos(\omega_1 t) & 0 \\ 0 & 0 & 1 \end{pmatrix}. \tag{2.4}$$

The angular velocities of the two motions are given by ω_1 (for revolution) and ω_2 (for rotation). If ρ is the ratio of the diameter of the o-ring's "track" cylinder to the diameter of the o-ring itself, then

$$\omega_2 = (1+\rho)\omega_1, \tag{2.5}$$

where the $(1+\rho)$ factor accounts for the single rotation that the sample would undergo for each revolution if fixed rigidly to the revolving arm.

The final equation of position for a given point on the substrate (ignoring the z component) is then

$$r' = R_1 T R_2 r, \tag{2.6}$$

or

$$x' = a\cos(\omega_1 t) + y[-\cos(\omega_2 t) * \sin(\omega_1 t) - \cos(\omega_1 t) * \sin(\omega_2 t)]$$
$$+ x[\cos(\omega_1 t) * \cos(\omega_2 t) - \sin(\omega_1 t) * \sin(\omega_2 t)], \tag{2.7}$$

and

$$y' = a\sin(\omega_1 t) + x[\cos(\omega_2 t) * \sin(\omega_1 t) + \cos(\omega_1 t) * \sin(\omega_2 t)]$$
$$+ y[\cos(\omega_1 t) * \cos(\omega_2 t) - \sin(\omega_1 t) * \sin(\omega_2 t)]. \tag{2.8}$$

For the computer program, the position on the sample is given in polar coordinates (r, ϕ). We call $\omega_1 t$ "θ" for the revolution position (the angle the arm holding the sample holder makes with

its original position above the target), and, making the $\omega_2 = (1+\rho)\omega_1$ substitution, we substitute "$(1+rho) * revpos$" for the rotation position $\omega_2 t$. The position equations for the program then become

$$x' = a\cos(\theta) + r\sin(\phi)\{-\cos[(1+\rho)\,\theta]\,\sin(\theta) - \cos(\theta)\,\sin[(1+\rho)\,\theta]\}$$
$$+ r\cos(\phi)\{\cos(\theta)\,\cos[(1+\rho)\,\theta] - \sin(\theta)\,\sin[(1+\rho)\,\theta]\} \tag{2.9}$$

and

$$y' = a\sin(\theta) + r\cos(\phi)\{\cos[(1+\rho)\,\theta]\,\sin(\theta) + \cos(\theta)\,\sin[(1+\rho)\,\theta]\}$$
$$+ r\sin(\phi)\{\cos(\theta)\,\cos[(1+\rho)\,\theta] - \sin(\theta)\,\sin[(1+\rho)\,\theta]\}. \tag{2.10}$$

Once the computer calculates the position of a point on the substrate, it finds the radial distance of the point from the center of the target. Assuming the target produces a radially symmetric deposition pattern on a stationary substrate, only the distance to the center of the target is needed to get a relative thickness or rate of deposition for that point in the vacuum chamber. The program looks up a thickness value from a curve fit of the actual deposition profile. This is added to the thickness being tallied for this point on the substrate. (Normalization will come in a moment.) This is essentially evaluating the path integral:

$$\int_{\theta_i}^{\theta_f} f \sqrt{\left(\frac{dx'}{d\theta}\right)^2 + \left(\frac{dy'}{d\theta}\right)^2}\, d\theta, \tag{2.11}$$

Where f is the thickness of a static profile as a function of radial distance from the center of the target (such as those given in Figure 2.9 and Figure 2.13). In this case, the integral simplifies to:

$$\int_{\theta_i}^{\theta_f} f \sqrt{a^2 + (x^2 + y^2)(2+\rho)^2 + 2a(2+\rho)\{x\cos[\theta(1+\rho)] - y\sin[\theta(1+\rho)]\}}\, d\theta. \tag{2.12}$$

Once the computer has followed a point on the substrate as it moves around the chamber, adding thickness values as it goes, the process is repeated for another point on the substrate, until values are given for all grid points on the substrate. The mean of all the thicknesses is taken and all thickness values are divided by the mean in order to normalize the data. As a measure of the sample's thickness uniformity, the smallest value is subtracted from the largest, and this number is also divided by the mean. I call this number the "Normalized Maximum Thickness Difference," or NMTD.

2.3.2   Optimal Parameters

In order to explore how the uniformity of our films might be affected by how many revolutions the planetary system makes, I ran the computer simulation over and over for varying numbers of revolutions, simulating a round substrate of radius 1 inch. Upon running the program out to 200 revolutions, I found that most of the interesting effects occur before 50 revolutions are completed, at which point the NMTD approaches a steady state limit. The program was iterated 491 times for each array profile, once for each number of revolutions from 1 to 50 in increments of 0.1. The resulting NMTD is plotted for Slide Array 2 in Figure 2.14 and for Slide Array 3 in Figure 2.15.

These plots may seem a bit surprising at first, especially that for Slide Array 3. We might expect the films to become monotonically more uniform as the number of revolutions increases. This is not the case. We can understand what is happening by looking at the paths followed by various points of the substrate as they travel around the chamber.

One noticeable feature of both plots is the decrease in uniformity occuring at about 5.8 revolutions. In order to explain why this occurs, let's describe the vacuum chamber using cartesian coordinates, with the center of the target and the initial position of the substrate located along the x-axis. We will take two points on edge of the substrate. (It's the edge that's most important in uniformity since the center of the rotating sample follows the same path every time.) The first starts

Array 2 Normalized Max Thickness Difference vs. No. of Revolutions
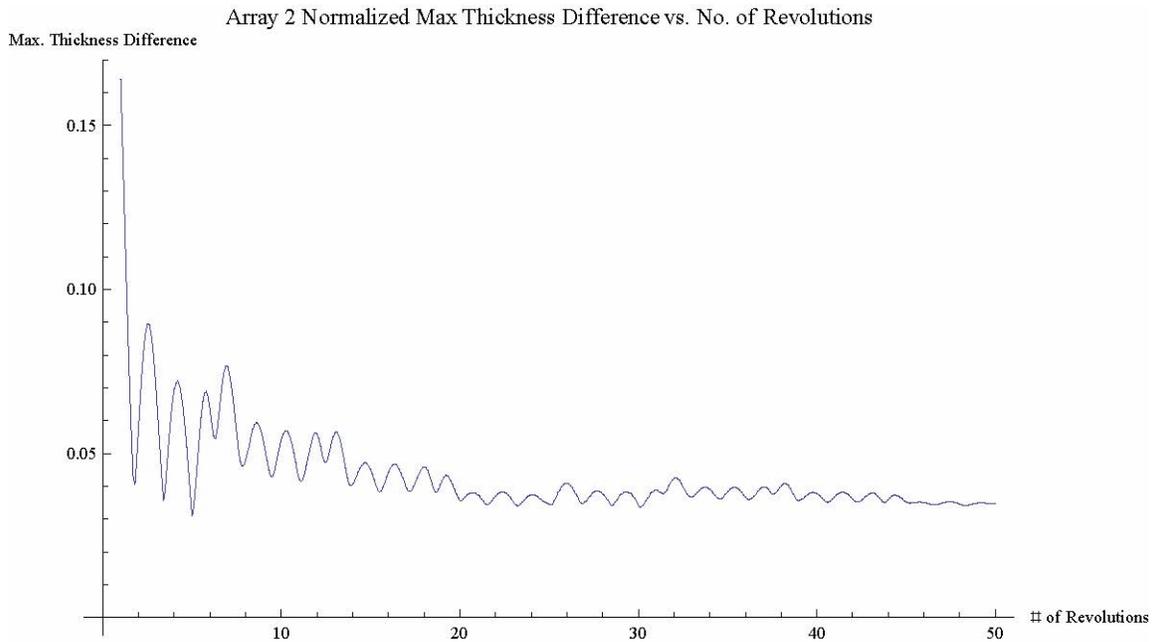
Figure 2.14 Predicted NMTD as a function of the number of revolutions completed by the planetary system, as predicted using the thickness profile of Array 2.

Array 3 Normalized Max Thickness Difference vs. No. of Revolutions
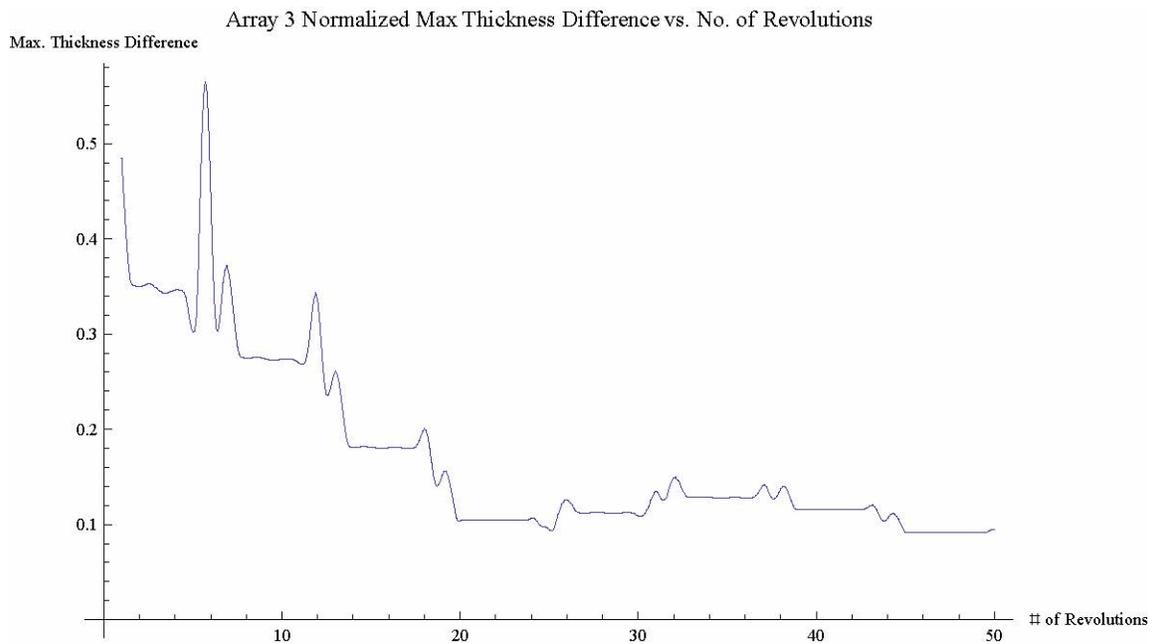
Figure 2.15 Predicted NMTD as a function of the number of revolutions completed by the planetary system, as predicted using the thickness profile of Array 3.

Path of Point (1 in. from Center of Sample) Through Vacuum Chamber: 5.8 Revolutions
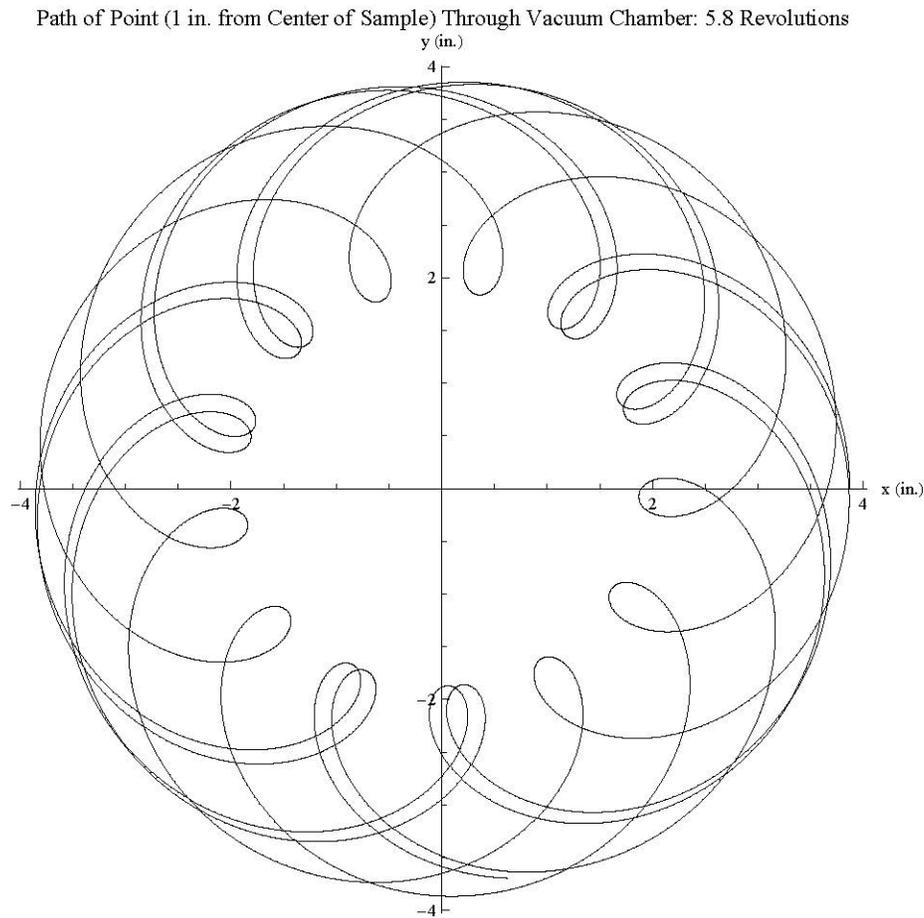
Figure 2.16 Path followed by a point located one inch from the center of the substrate's rotation. At this point the planetary system has completed 5.8 revolutions. This point starts at (3.87, 0), which is the edge of the 1-inch diameter substrate which is farthest from the center of the chamber. Notice the locations of the double loops.

at one inch to the right of the substrate's center; the second starts one inch to the left. Following point number one for 5.8 revolutions, we get Figure 2.16. Following the second path, we get Figure 2.17.

We see that at this moment in the revolution of the planetary, Point 1 has followed looped around the chamber, but has nearly repeated certain parts of its path. We see double loops in certain parts of the pattern, arranged nearly in an equilateral triangle pointing downward towards negative y. When we look at the pattern produced by Point 2, we see the same pattern, but inverted,

Path of Point (1 in. from Center of Sample) Through Vacuum Chamber: 5.8 Revolutions
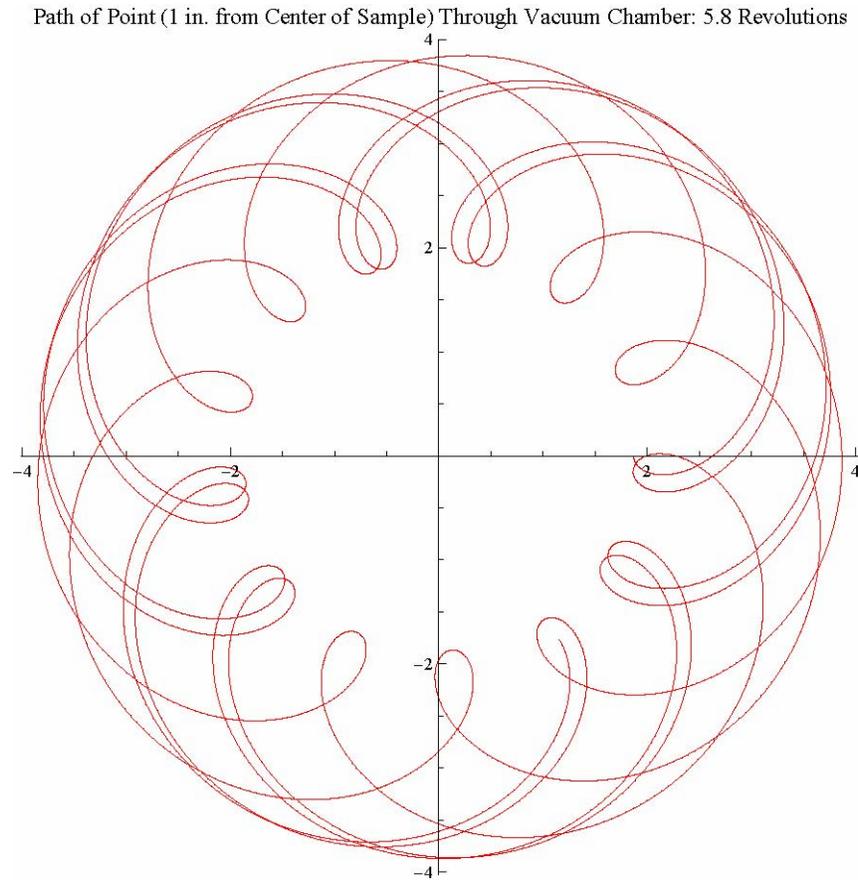
Figure 2.17 Path followed by a point located one inch from the center of the substrate's rotation. At this point the planetary system has completed 5.8 revolutions. This point starts at (1.87, 0), on the starting point of the substrate nearest the chamber. Compare the locations of the double loops for this point with those for the previous point in Figure 2.16.
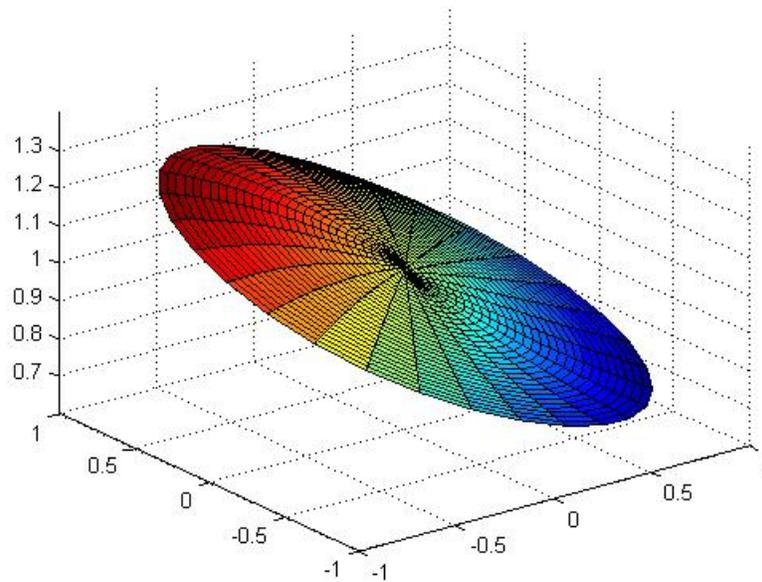
Figure 2.18 Predicted normalized film thickness (1 is the mean value) for a sample sputtered under the conditions of Array 3 with 5.8 revolutions, a number of revolutions chosen for large NMTD. The horizontal x and y axes are given in inches.

with the imaginary triangle pointing up. This is a moment during the revolution when the general areas where a point spent time in the chamber is strongly influenced by the point's location on the substrate. For a target centered on the planetary's revolution axis, this would not be much of a problem, but for an offset target with a very sharply peaked deposition profile such as that for Array 3, this becomes a significant issue. We can see just what is happening to the film at this point in Figure 2.18. One side of the film has been spending more time in a region of significantly more flux.

Similar stories can be told for samples sputtered at the distance of Array 2 at 3 revolutions (Fig. 2.19), and those sputtered at the Array 3 distance at 11 revolutions (roughly double 5.8 revolutions), shown in Figure 2.20. All of these points roughly correspond to local maxima for the NMTD.
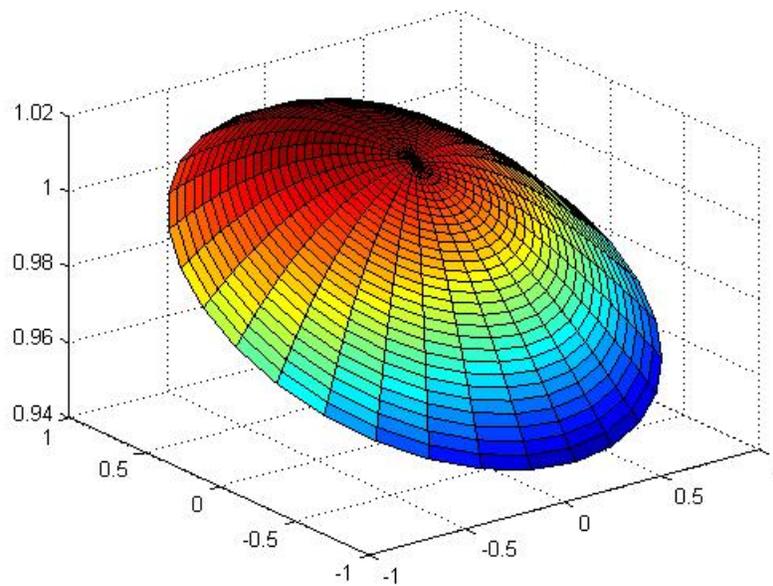
Figure 2.19 Predicted normalized film thickness (1 is the mean value) for a sample sputtered under the conditions of Array 2 with 3 revolutions, giving a relatively large NMTD. The horizontal x and y axes are given in inches.
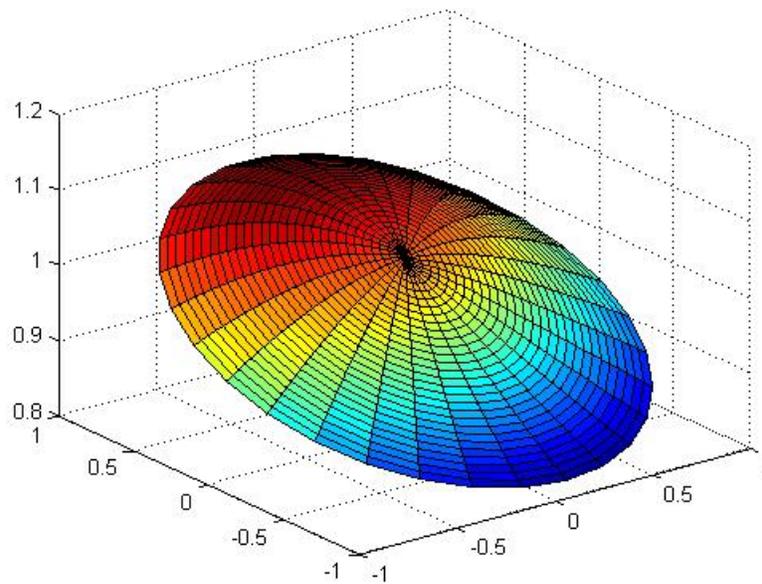
Figure 2.20 Predicted normalized film thickness (1 is the mean value) for a sample sputtered under the conditions of Array 3 with 11 revolutions, showing another relatively large NMTD. The x and y axes are given in inches (horizontal axes).

Path of Point (1 in. from Center of Sample) Through Vacuum Chamber: 25 Revolutions
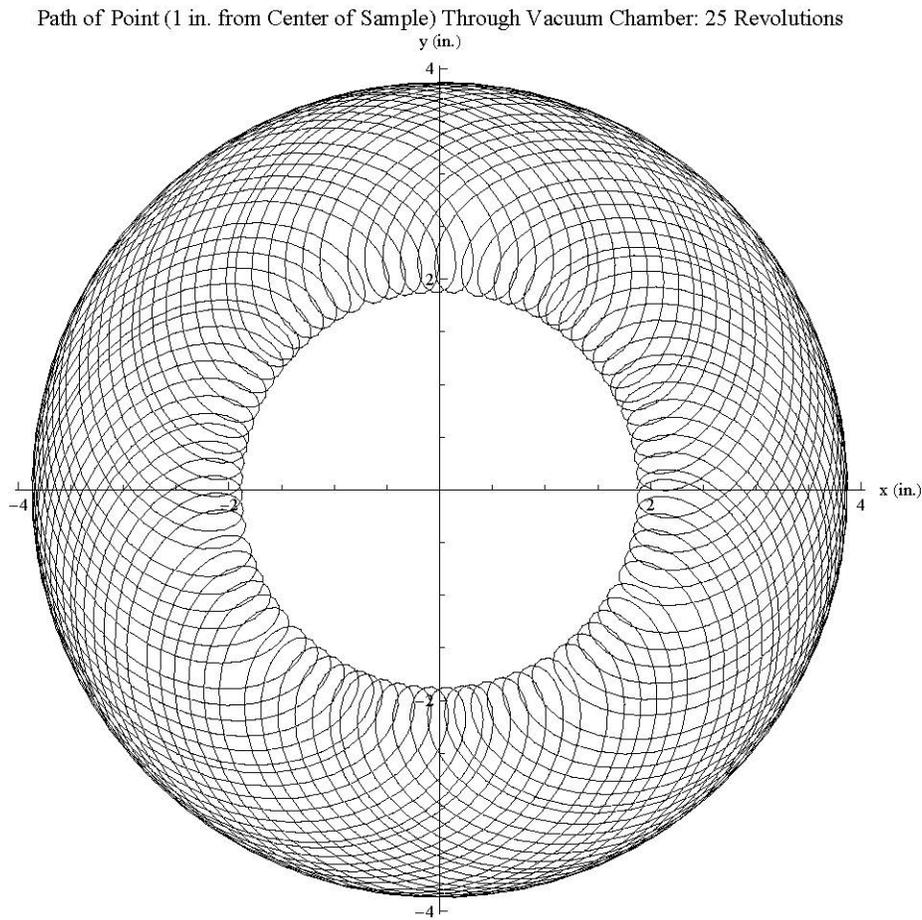
Figure 2.21 Path followed by a point located one inch from the center of the substrate's rotation. At this point the planetary system has completed 50 revolutions and the NMTD is nearing a minimum.

There is hope, however. Once the sample under deposition has completed enough revolutions to have spent roughly equal portions of its time in each sector of the vaccuum chamber, all points on the sample will have followed a similar pattern and received nearly equal deposition. This is the case at about 25 revolutions (see Fig. 2.21).

After the samples complete this initial full sweep of the vacuum chamber, they repeat the pattern from their new starting position. This causes continued fluctuations, but because the sample average now includes large amounts of previously deposited material, the effect of further fluctuations on the overall mean decreases with each full cycle. By about 50 revolutions, the NMTD's of
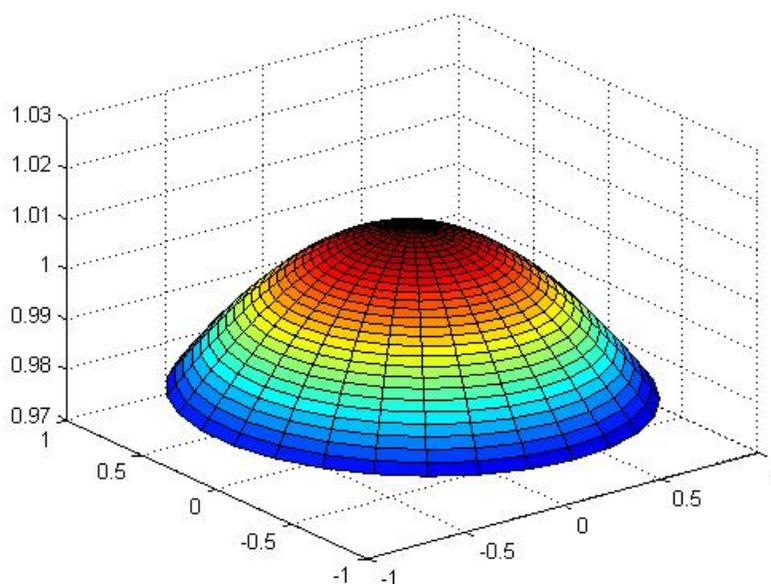
Figure 2.22 Predicted normalized film thickness (1 is the mean value) for a sample sputtered under the conditions of Array 2 with 50 revolutions. The horizontal x and y axes are given in inches.

the samples are nearing a minimum limit, as compared to simulations run out to 200 revolutions.

Films sputtered through 50 revolutions are simulated in Figure 2.22 for the Array 2 profile (farther from the target) and for the Array 3 profile (very close to the target) in Figure 2.23. Note that for these simulations, which produced lower NMTD's, the maxima of the deposition profiles are located closer and closer to the center of the the sample's rotation, which is what we would expect.

2.4 Testing the Computer Predictions

2.4.1 Deposition Parameters

A sample (named Sample 120724) was prepared on July 24, 2012 which was susequently measured and checked against the predicted film thickness profile. A uranium oxide film was sputtered on
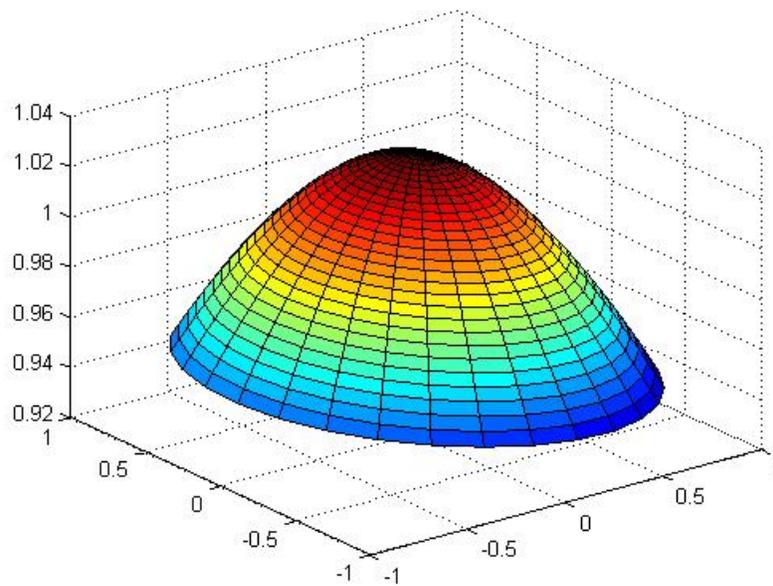
Figure 2.23 Predicted normalized film thickness (1 is the mean value) for a sample sputtered under the conditions of Array 3 with 50 revolutions. The horizontal x and y axes are given in inches.
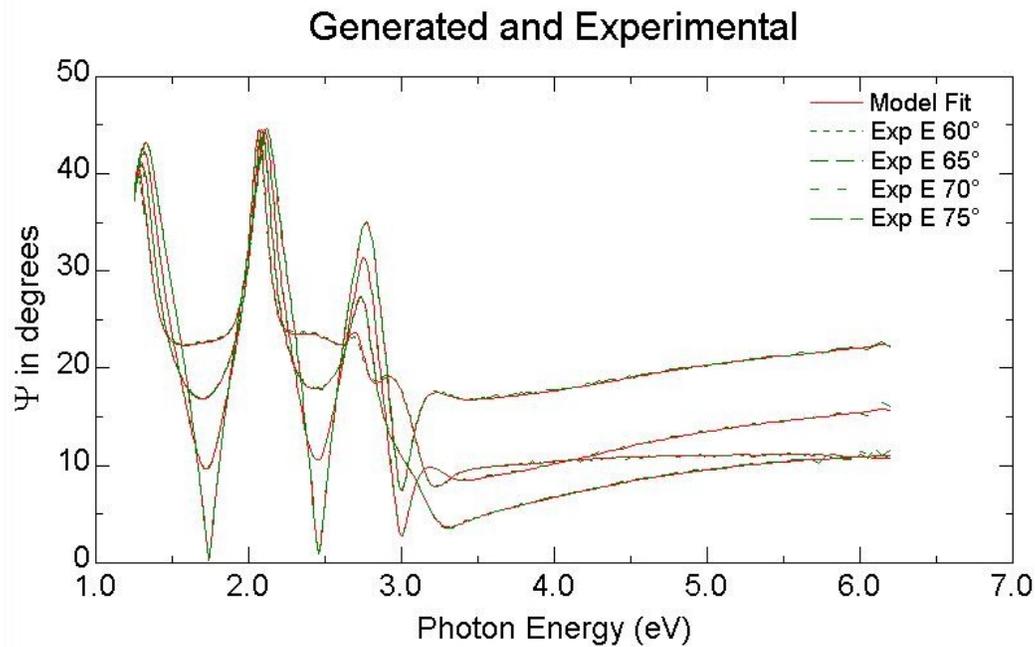
Figure 2.24 Ellipsometric measurement Ψ relative to photon energy (eV) for four angles for a point on Sample 120724.

a silicon wafer held approximately 14 cm (5.5 inches) above the uranium target. Total pressure was maintained near $6.53*10^{-4}$ torr. The partial pressure of oxygen was 42%. Sputtering was maintained for 135 minutes.

2.4.2 Characterization

Sample 120724 was characterized using ellipsometry but not transmission (Si substrate). Ellipsometric measurements were taken at 0.1-inch intervals in a radial direction from near the center of the sample's rotation. An example of Ψ is given in Figure 2.24. Ten of these points, each with data taken at four angles, were used to constrain the films thickness (Fig. 2.25) and optical and dielectric constants (Fig. 2.26 and Fig. 2.27). The profile of the film appears to be very similar to the shape suggested by the computer program.
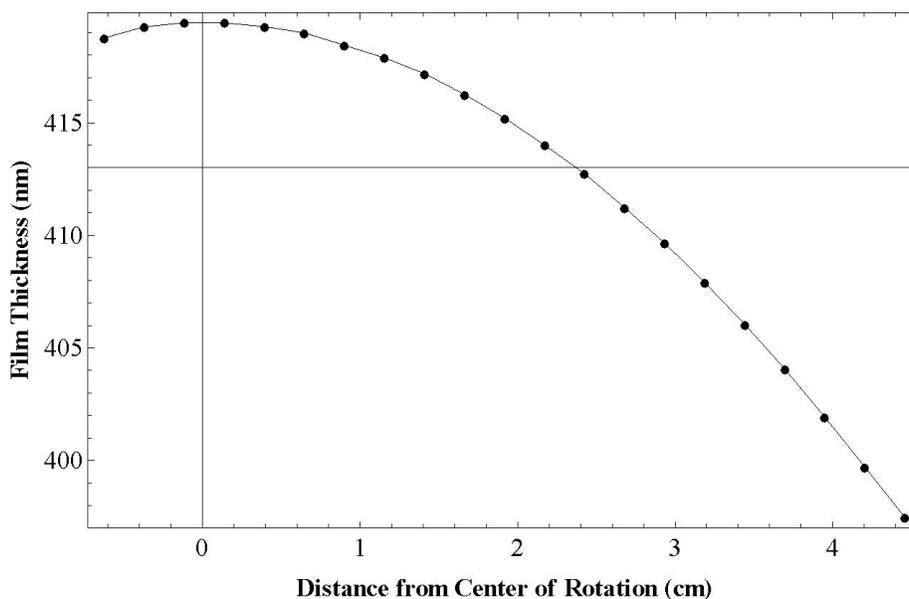
Figure 2.25 Sample 120724 film thickness as a function of radial distance from the center of the deposition profile. The center of the profile was determined by symmetry and nearly corresponds to the center of rotation for the substrate holder. Note that the horizontal axis is given in centimeters rather than inches.
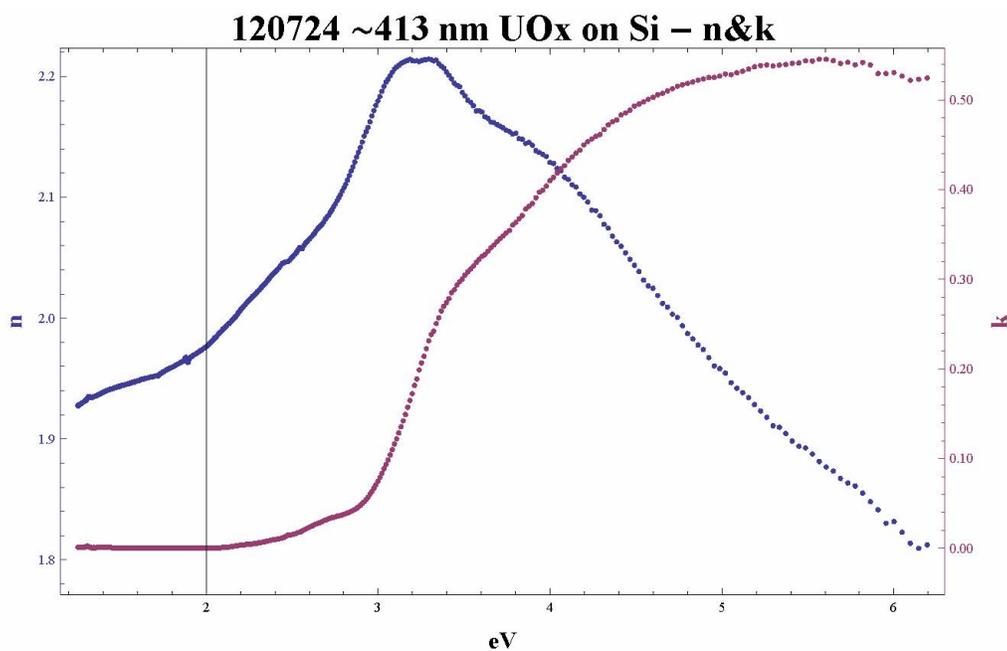

Figure 2.26 Optical constants n and k for Sample 120724 as a function of photon energy (eV).
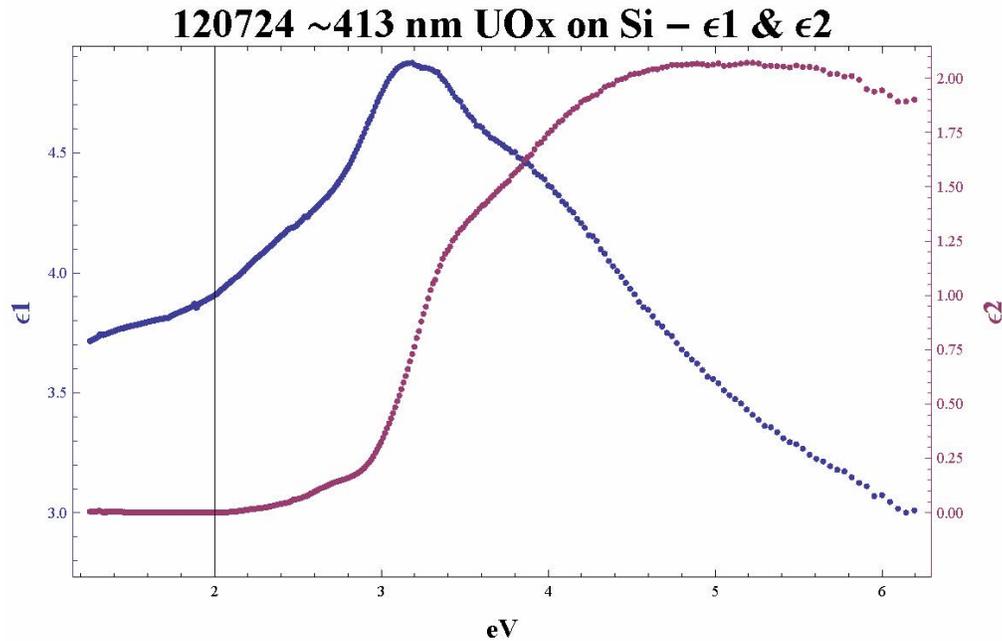
Figure 2.27 Dielectric constants ε_1 and ε_2 for Sample 120724 as a function of photon energy (eV).

2.4.3 Comparsion to Computer results

While the shape of the deposited film is similar to that predicted, by finding the average thickness for an area of Sample 120724 and multiplying it by the normalized thickness of a simulated film, we can better judge the accuracy of the computer predictions. In Figure 2.28, this is done for a one-inch radius sample centered at the radius of rotation for the sample holder. We expected that using the profile of Array 2 would be more accurate, since the films were sputtered at similar distances from the target, and this proves to be the case.

The actual film is even more uniform than the computer model would suggest, having a Normalized Maximum Thickness Difference of 0.0160. We don't know why this is. While there is slippage between the o-ring and its track, it is unlikely that this would cause much of a difference after several dozen revolutions. Another possibility is that Sample 120724 was not measured exactly along its diameter, but rather along some chord near the diameter. However, if the profiles are
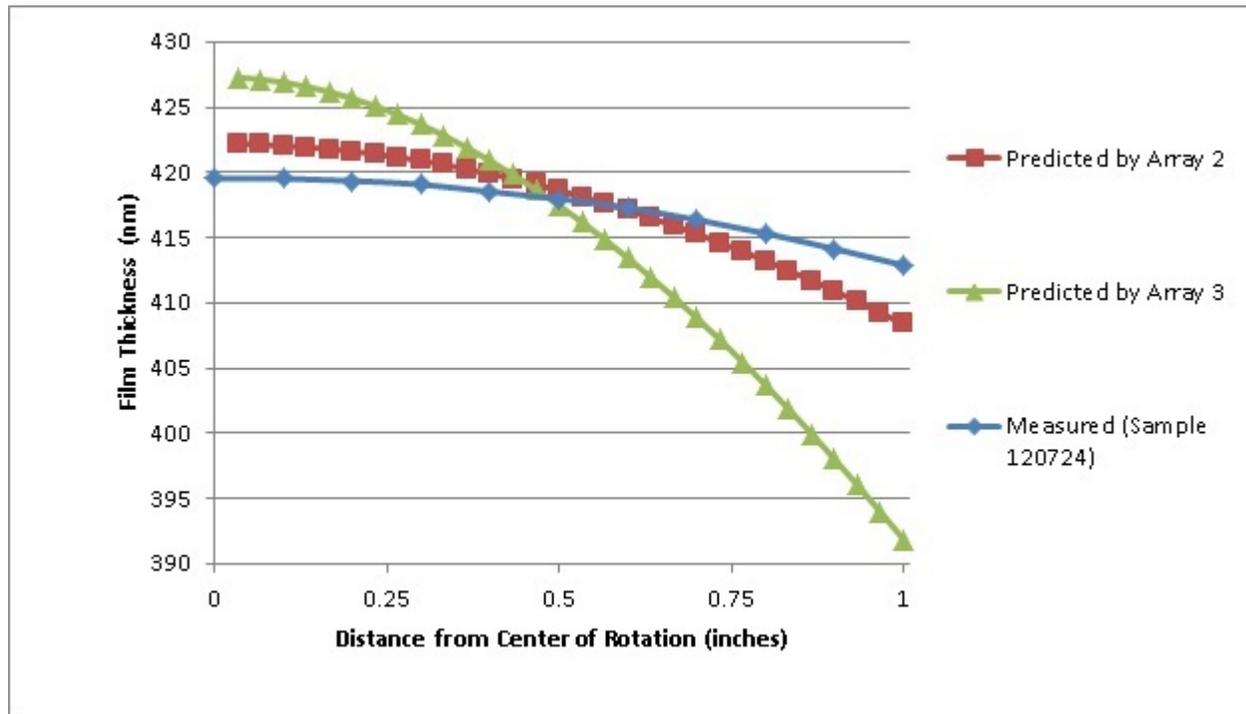
Figure 2.28 Thickness profiles as functions of radial distance from center of rotation as predicted using Array 2 profile and Array 3 profile and as measured for Sample 120724.

assumed to tend to symmetrical parabloids of revolution, as they appear to, this would not affect the shape of the deposition profile, but only its total thickness, actually *increasing* the NMTD.

It is possible that the steady state limit of minimum NMTD is actually lower than predicted. The stepper motor causing the planetary system to revolve made a complete turn about once every 20 seconds, leading to approximately 400 revolutions, far beyond any simulations I made. While the NMTD should not approach zero (unless the average flux per revolution intercepted at every point happens to be the same as the average intercepted at the center of rotation), such a large number of revolutions may lead to this greater uniformity.

Chapter 3

Conclusion

Making uniform thin films is still a daunting challenge. It remains to be seen whether our system will be able to consistently produce uniform films that are only tens of nanometers thick, as needed for multilayer mirrors effective in the EUV range. However, the percent variation in our films has dropped by about an order of magnitude since the installation of the planetary system.

The computer model developed for the deposition profile appears to be adequate for our purposes, provided that it is supplied with reliable data to begin with. It also appears that the computer model may tend to underestimate the uniformity of the actual films. Future work may be done to further characterize the sputtering profile for other various distances from the target. Valuable information may also be obtained by considering positions for the substrate other than centered on the rotation axis as we have described here, though such depositions may not give greater uniformity while requiring the substrate holder to stay within the confines of the vacuum chamber.

While highly advanced, involved, and expensive methods exist for producing extremely uniform films, our research shows that reasonably uniform films can be produced with relatively simple system.

Appendix A

MATLAB Code

```
clear all;

close all;

%

%using data from sample grown 4 cm from target

%switch to other depfit function to simulate sample grown

%about 5 inches from target

%measurements are in inches

numtestrevs = 491;

testrevmin = 1;

testrevmax = 50;

dtestrev = (testrevmax-testrevmin)/(numtestrevs-1);

testrev = testrevmin:dtestrev:testrevmax;
```

```
params = zeros(1,length(testrev));

for revtest = 1:numtestrevs,



N = 30; %number of radial points across the sample

M = 30; %number of angles around the sample



sr = 1; %radius of the sample

revtot = testrev(revtest); %total revolutions run

L = 30*revtot; %number of revolution steps

thick = zeros(N,M); %start with thickness of zero across sample



%Array 2 profile fitting function

%depfit = @(x) 34.6316 + 0.702627.*x - 4.90448.*x.^2 + 1.45603.*x.^3

% - 0.174891.*x.^4 + 0.00748875.*x.^5 ;

%function to fit the deposition profile (radially out from center of target)



%Array 3 profile fitting function

depfit = @(x) 1284.03 + 56.9532.*x + 76.9681.*x.^2 - 476.965.*x.^3

+ 291.307.*x.^4 - 80.9429.*x.^5 +12.4174.*x.^6 - 1.08878.*x.^7

+ 0.0512703.*x.^8 - 0.00100792.*x.^9;

%function to fit the deposition profile (radially out from center of target)



R = 2.87; %radius to center of revolution
```

```
Rt = 3.375; %distance from center of target to center of revolution

rho = 2.26; %ratio of large "gear" to small "gear"

th0 = 0; %initial angle of the revolution (zero is the position of the target)


rmin = 0;  %setting up the grids

rmax = sr;

dr = (rmax-rmin)/(N-1);

r = rmin:dr:rmax;


phimin = 0;

phimax = 2*pi;

dphi = (phimax-phimin)/(M-1);

phi = phimin:dphi:phimax;


revmin = 0;

revmax = revtot;

drev = (revmax-revmin)/(L-1);

rev = revmin:drev:revmax;




for n = 1:N,

    rpos = n*dr;

    for m = 1:M,

        phipos = m*dphi;
```

```
        for l = 1:L;

        revpos = l*drev;

        xpos = R*cos(revpos)+rpos*sin(phipos)*(-cos((1+rho)*revpos)*sin(revpos)

                -cos(revpos)*sin((1+rho)*revpos))

              +rpos*cos(phipos)*(cos(revpos)*cos((1+rho)*revpos)

               -sin(revpos)*sin((1+rho)*revpos));

        ypos = R*sin(revpos)+rpos*cos(phipos)*(cos((1+rho)*revpos)*sin(revpos)

                +cos(revpos)*sin((1+rho)*revpos))

              +rpos*sin(phipos)*(cos(revpos)*cos((1+rho)*revpos)

               -sin(revpos)*sin((1+rho)*revpos));

        dist = ((xpos-Rt)^2+ypos^2)^(1/2);


        thick(n,m) = thick(n,m)+depfit(dist);

        end


    end


end


[theta,rho] = meshgrid(phi,r);
[X,Y] = pol2cart(theta,rho);


mx = max(max(thick));
thicknorm = thick/mean(mean(thick)); %normalize the thickness data so
                                 %we get relative thickness
```

```
%figure

%surf(X,Y,thicknorm)


%normstddev = std2(thicknorm)


 mn = min(min(thick));

 av = mean(mean(thick));

 varypercent =(mx-mn)/av

 params(revtest) = varypercent;


% figure

% q = 0:.1:6;

% plot(depfit(q)

end


plot(testrev,params)
```

Bibliography

Squires, M. B. 1999, On Determining the Optical Constants of Sputtered U and a-Si at 304 and

  584 Angstroms

Wehner, G. K., & Rosenberg, D. 1960, Journal of Applied Physics, 31, 177